JOURNAL OF MATERIALS SCIENCE 27 (1992) 5339–5342

Interactions between nickel and melted R–Ba–Cu–O (R=Y, Nd)

D. DUBÉ, P. LAMBERT, B. CHAMPAGNE
Industrial Materials Institute, National Research Council of Canada, 75 Boul. de Mortagne, Boucherville, Québec, Canada J4B 6Y4

R–Ba–Cu–O (R = Y and Nd) compounds were melted and crystallized in nickel crucibles. The interaction between these materials was studied by examining the physical aspect of the nickel interface. Interaction mechanisms between nickel and melted R–Ba–Cu–O compounds are proposed to explain the formation of an interface, constituted of a top layer of $Ni_{0.8}Cu_{0.2}O_x$ and of an NiO_x underlayer as well as the presence of nickel oxide-rich particles in the melt.

1. Introduction

Interaction of R–Ba–Cu–O melt with materials impedes the processing and the crystal growth of these superconductors [1–6]. The interactions of R–Ba–Cu–O melts with metals or alloys need to be better understood for producing metal/HTSC composite conductors involving directional solidification. Among metals, nickel has appeared to be an interesting candidate for solid-state consolidation of $RBa_2Cu_3O_x$ such as hot-isostatic pressing [6] as well as melting [4]. Even though some nickel is dissolved by Y–Ba–Cu–O melts [4–7], the decrease of the critical temperature of $YBa_2Cu_3O_x$ is not as severe as that of many other metallic atoms. For example, nickel concentrations below about 3 at % lead to a transition temperature of about 77 K whereas the same content of cobalt or iron pushes the transition below the liquid nitrogen boiling point [8–13].

This paper reports a study of the interaction between nickel and R–Ba–Cu–O (R = Y, Nd) melts and assesses phase composition and the nickel contamination mechanisms of the melt.

2. Experimental procedure

Pellets were prepared from mixtures of Y_2O_3 or Nd_2O_3 (each 99.999% pure), $BaCO_3$ (99.9% pure) and CuO (99.999% pure) powders. Two different R-based (Y or Nd) compositions were mixed in R:Ba:Cu/1:4:18 molar proportion. These two mixtures were pressed and then sintered at 900–930 °C (Y–Nd) for 36 h in air with intermediate grindings.

About 10 g R–Ba–Cu–O of each composition were placed in a 0.5 mm thick nickel crucible (chemical composition listed in Table I). Crucibles were heated at about 50–100 °C min^{-1} to the melting temperature for 900 s, and were then rapidly cooled by immersing the bottom of the crucible in cold water (Fig. 1). The resulting Y–Ba–Cu–O and Nd–Ba–Cu–O compounds were then subjected to a slow crystallization process from 920 and 1020 °C, respectively.

Phase composition near the interface was assessed by scanning electron microscopy (SEM) using energy dispersive spectroscopy (EDX).

3. Results and discussion

3.1. Microstructure after quenching

Rapidly cooled Y–Ba–Cu–O compound (Fig. 2) is constituted of a fine solidification microstructure con-

TABLE I Chemical composition of the nickel crucibles (wt %)

Ni	Mn	Fe	Mg	Si	C	Cu	S
99.53	0.22	0.09	0.06	0.04	0.03	0.01	0.003

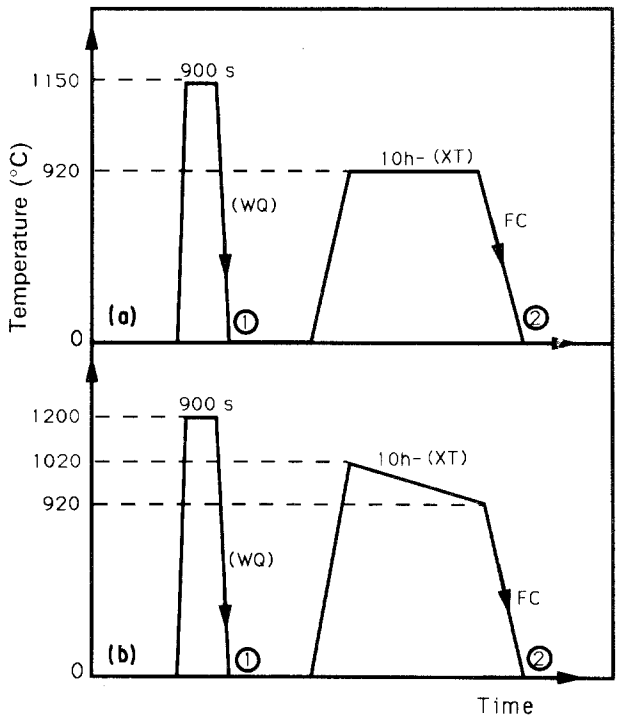

Figure 1 Thermal treatments: (a) Yttrium-based compounds, (b) neodymium-based compounds. WQ, XT and FC stand for water quenching, crystallization and furnace cooling, respectively.

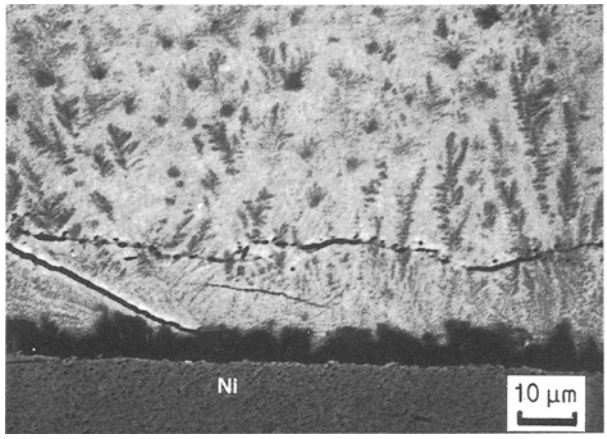

Figure 2 Scanning electron micrograph of the Y–Ba–Cu–O melt after rapid cooling.

taining nickel oxide dendrites which indicates that complete melting occurred. The main orientation of the primary arms of the nickel oxide dendrites is perpendicular to the crucible wall which is the direction of the thermal gradient. Quenching rates were relatively high because the secondary dendrite arm spacing of the nickel oxide dendrites is about 1 μm.

The microstructure of the Nd–Ba–Cu–O compound consists essentially of primary $Nd_3Ba_3Cu_6O_x$ crystals enclosing small nickel oxide pure cuboids in a matrix constituted of a fine Ba–Cu–O eutectic network. It should be mentioned that the $Nd_3Ba_3Cu_6O_x$ crystals were formed from the melt because they were not present in the precursors. The relative size of the 336 phase suggests that this phase was formed before quenching (Fig. 3a, b).

After rapid cooling, the reaction zones between the melt and the crucible are continuous and about 5–10 μm thick for Y–Ba–Cu–O compounds (Fig. 2). They are discontinuous and about 10–20 μm thick for Nd–Ba–Cu–O compounds (Fig. 3a). It is worth mentioning that the rapidly cooled Nd–Ba–Cu–O ingot contained clouds of small nickel oxide cuboids (Fig. 3b). Their presence in the melt after such a short melting period at 1200 °C suggests that part of the nickel oxide layer formed on the crucible was probably smashed to angular fragments in the melt. Moreover, the non-uniform distribution of the cuboids in the melt also indicates that their formation by a precipitation mechanism during the rapid cooling process is unlikely, because in such a case they would have been more evenly dispersed.

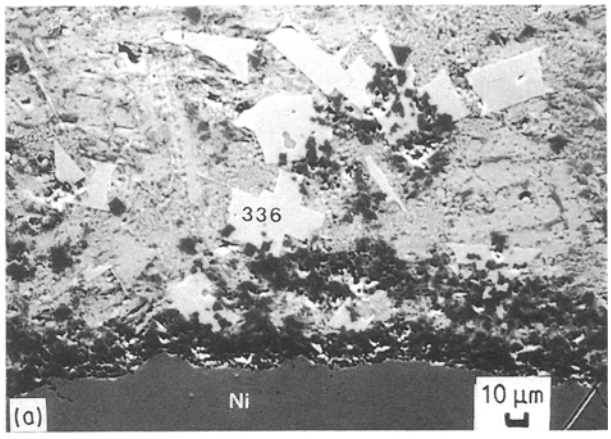

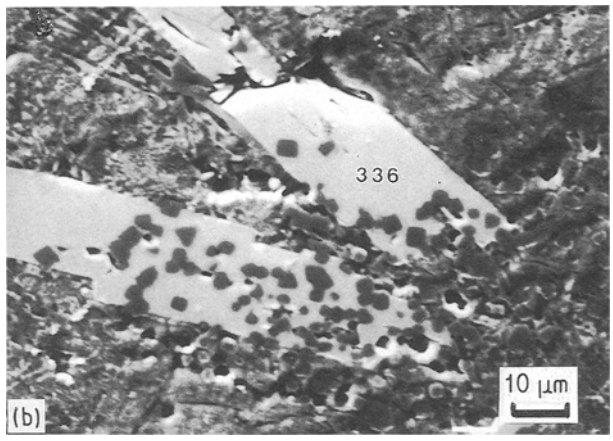

Figure 3 (a) Scanning electron micrograph of the Nd–Ba–Cu–O melt after rapid cooling. (b) Nickel oxide-rich cuboids dispersed in the melt.

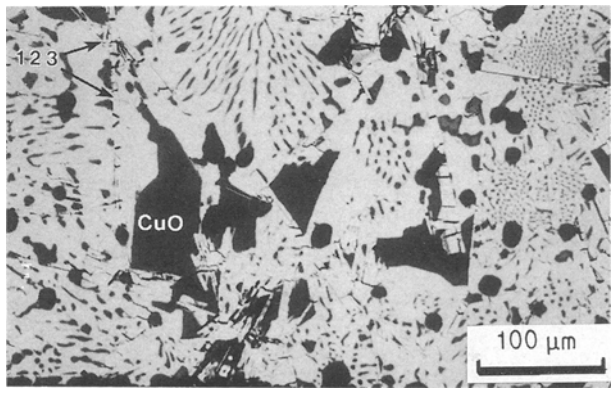

Figure 4 Scanning electron micrograph of the Y–Ba–Cu–O ingot after crystallization.

3.2. Microstructure after crystallization

The crystallization cycle led to a significant modification of the microstructure of quenched ingots. For the Y–Ba–Cu–O compound, massive CuO_x phases containing about 1 at % Ni and $Y_1Ba_2(Cu,Ni)_3O_{7-\delta}$ platelets were enclosed in a fine $BaCuO_x$–CuO_x eutectic (Fig. 4). Nickel oxide dendrites of the rapidly cooled ingots disappeared during crystallization. Furthermore, a dispersion of spheroids of about 10–50 μm diameter was found in the melt. The composition of these spheroids corresponds to $Ni_xCu_{1-x}O$ where x ranges between 0.7 and 0.8.

For the Nd–Ba–Cu–O compound, the microstructure consists of CuO_x phases and of two types of $Nd_xBa_y(Cu,Ni)_zO_\delta$ compounds with a $x:y:z$ stoichiometry corresponding to 1:2:3 and 3:3:6 embedded in a $BaCuO_x$–CuO_x eutectic (Fig. 5). The presence of these two ternary phases in the solidified Nd–Ba–Cu–O ingot is in accordance with phase equilibrium diagrams of R–Ba–Cu–O with large R atoms [14–16]. Similar to Y–Ba–Cu–O, less than 1 at % Ni

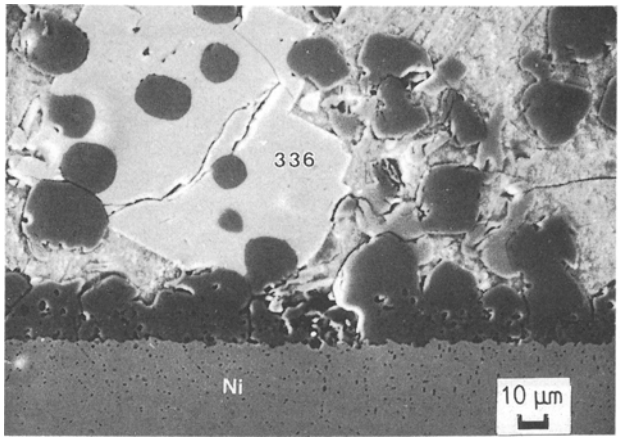

Figure 5 Scanning electron micrograph of the Nd–Ba–Cu–O ingot after crystallization.

was found in the CuO_x phases. This low nickel concentration observed in the CuO_x phase is in agreement with data reported on the NiO–CuO system [17]. The nickel oxide cuboids observed after quenching the Nd–Ba–Cu–O ingots disappeared during the crystallization but nickel-rich spheroids of 10–50 μm diameter were present in the Nd–Ba–Cu–O melt after crystallization. Their composition corresponds to $Ni_xCu_{1-x}O_z$ with x ranging between 0.7 and 0.8 which is identical to the composition of the spheroids of the Y–Ba–Cu–O melt.

The physical aspect of the interface zone and the corresponding copper and nickel elemental mappings clearly reveal a significant reaction between the melt and the crucible (Fig. 6a–c). The interface is about 20 μm thick and is divided in two zones: a top layer consisting of dense nickel–copper oxide protuberances and a continuous and porous nickel oxide underlayer growing on nickel. The stoichiometry of the top layer corresponds to $Ni_wCu_{1-w}O_z$ with $0.70 < w < 0.85$ whereas the underlayer contains no copper. Neither R atoms nor the barium atom was detected in the interface layers. It is worthy of note that the nickel in the vicinity of the nickel oxide underlayer contains voids and inclusions in the grains as well as at grain boundaries. These inclusions are manganese-rich but their exact composition could not be assessed owing to their small size.

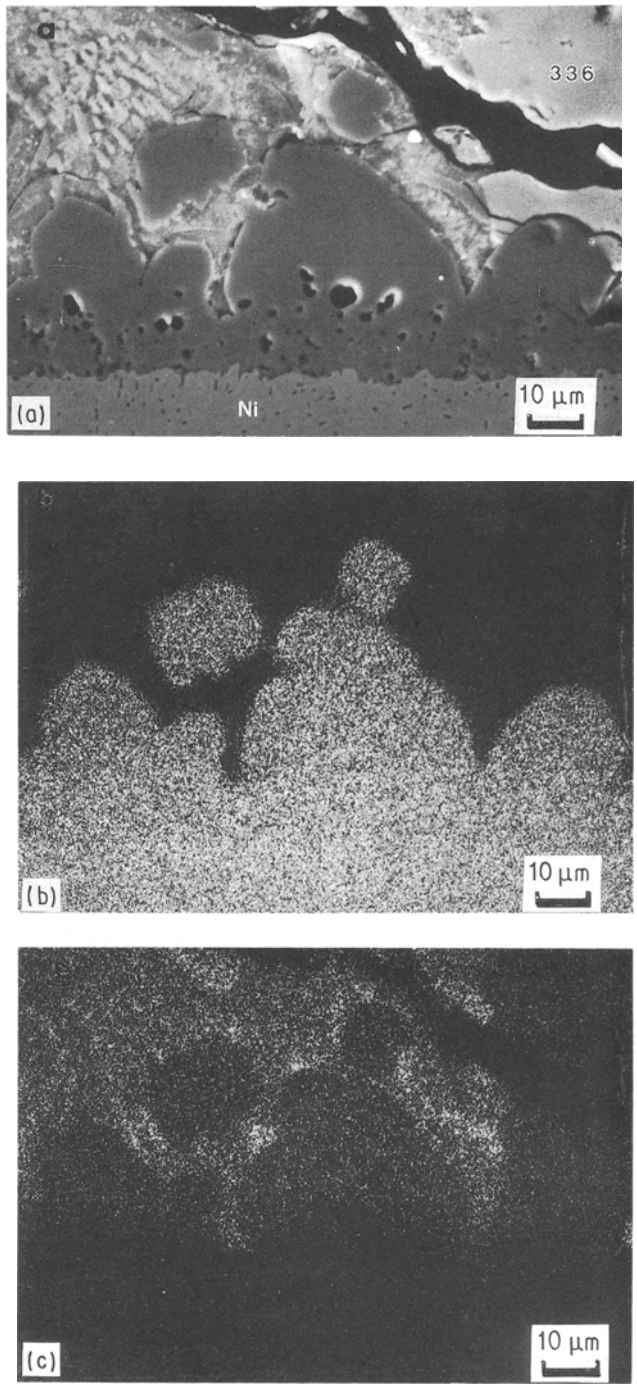

Figure 6 (a) Scanning electron micrograph of the interface zone for the Nd–Ba–Cu–O ingot after rapid cooling and crystallization showing the NiO underlayer and the $Ni_wCu_{1-w}O_z$ top layer. (b) Nickel X-ray mapping. (c) Copper X-ray mapping.

3.3. Formation of nickel-rich spheroids in the melt

A schematic illustration of the formation mechanism of the nickel-rich spheroids, referred to as a growth and detachment mechanism, is depicted in Fig. 7. Nickel atoms diffused from the nickel wall through the nickel oxide reaction layer and combined with the oxygen atoms of the melt leading to the growth of this layer [18]. In this particular type of diffusion, voids are formed near the Ni/NiO interface due to metal vacancies. Indeed this phenomenon has been reported for the oxidation of nickel alloys of commercial purity [18–20]. Because the nickel atom is quite mobile in the nickel oxide reaction layer and its diffusion leaves an increasing concentration of nickel vacancies, voids are generated in the nickel near the Ni/NiO interface. On the melt side, copper atoms diffuse from the R–Ba–Cu–O melt in the oxide layer and substitute for nickel atoms. The expansion caused by the insertion of copper atoms in the nickel oxide structure [21] creates tensile stresses in the nickel oxide underlayer promoting the growth and coalescence of the pores in the nickel oxide layer similar to the oxidation of nickel in oxygen atmospheres [18]. This coalescence process leads to a separation of the Ni–Cu–O protuberances from the underlayer which are then dispersed by the

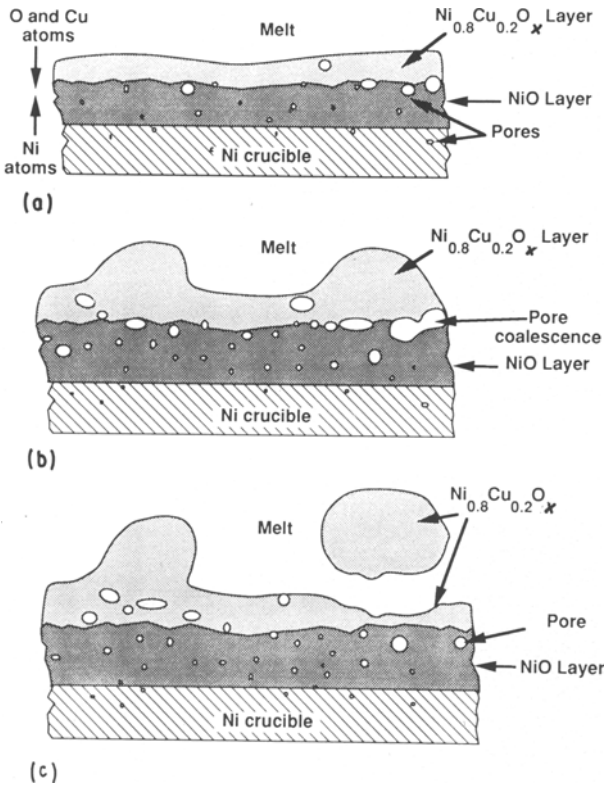

Figure 7 Schematic of the formation of spheroids according to the growth and detachment mechanism. (a) Diffusion of oxygen, nickel and copper through the interface. (b) Growth of the $Ni_wCu_{1-w}O_z$ top layer. (c) Coalescence of pores, detachment and dispersion of protuberances.

natural convection flow of the melt. The nearly equivalent size of the spheroids suggests that they are in equilibrium with the melt at these temperatures.

After the crystallization cycle, $Nd_3Ba_3(Cu,Ni)_6O_\delta$ crystals still enclosed an Ni–Cu–O phase which spheroidized due to an important diffusion of copper during the crystallization (Fig. 5). The composition of these spheroids is $Ni_xCu_{1-x}O_z$ with x ranging between 0.7 and 0.8.

Additional experiments conducted with Er–Ba–Cu–O compounds under conditions identical to those of Y–Ba–Cu–O compounds yielded the same microstructure consisting of a dispersion of nickel–copper spheroids after the crystallization cycle as that observed for the neodymium and yttrium compounds. It can be suggested that the interaction of R–Ba–Cu–O melt with nickel, for R different from yttrium, neodymium or erbium, is likely to be similar to that observed in this work.

4. Conclusion

R–Ba–Cu–O compounds (R = Nd, Y) were melted rapidly cooled and then slowly crystallized in nickel crucibles. At the interface, a reaction zone consisting of a nickel–copper oxide top layer and a nickel oxide underlayer was observed. A mechanism based on the formation and detachment of protuberances was proposed to explain the contamination of the melt by Ni–Cu–O spheroids. Moreover, the nickel substitution for copper led to the crystallization of quaternary nickel-doped 123 and 336 phases. The similarity of the interaction noted with R–Ba–Cu–O (R = Er, Nd and Y) suggests that the reaction between nickel and R–Ba–Cu–O is likely to be similar for other R atoms.

References

1. D. L. KAISER, F. HOLTZBERG, B. A. SCOTT and T. R. McGUIRE, *Appl. Phys. Lett.* **51** (1987) 1040.
2. X. Z. ZHOU, A. H. MORRIS, J. A. EATON, M. RAUDSEPP and Y. L. LUO, *J. Appl. Phys.* **20** (1987) 1542.
3. H. J. SCHEEL and F. LICCI, *MRS Bull.* **XIII** (1988) 56.
4. H. SCHLÜTER and H.-J. GÜNTHERODT, *Phys. C* **153–155** (1988) 383.
5. H. J. SCHEEL, W. SADOWSKI and L. SCHELLENBERG, *Supercond. Sci. Technol.* **2** (1989) 17.
6. B. CHAMPAGNE, L. PARENT and C. MOREAU, *ibid.* **2** (1989) 25.
7. P. LAMBERT, D. DUBÉ, B. ARSENAULT and B. CHAMPAGNE, *Thin Solid Films*, **193** (1990) 847.
8. J. M. TARASCON, L. H. GREENE, P. BARDOUX, W. R. McKINNON, G. W. HULL, T. P. ORLANDO, K. A. DELIN, S. FONER and E. J. McNIFF Jr, *Phys. Rev. B* **36** (1987) 8393.
9. GANG XIAO, F. H. STREITZ, A. GAVRIN, Y. W. DU and C. L. CHIEN, *ibid.* **35** (1987) 8782.
10. Y. MAENO, T. NOJIMA, Y. AOKI, M. KATO, K. HOSHINO, A. MINAMI and T. FUJITA, *Jpn J. Appl. Phys.* **26** (1987) L774.
11. M. F. YAN, W. W. RHODES and P. K. GALLAGHER, *J. Appl. Phys.* **63** (1988) 821.
12. Z. H. HE, Z. Y. CHEN, J. S. XIA, G. Q. PAN, Y. T. QIAN and Q. R. ZHANG, *ibid.* **64** (1988) 3589.
13. J. F. BRINGLEY, T.-M. CHEN, B. A. AVERILL, K. M. WONG and S. J. POON, *Phys. Rev. B* **38** (1988) 2432.
14. S. A. HODOROWICZ, A. LASOCHA, W. LASOCHA and H. A. EICK, *J. Solid State Chem.* **75** (1988) 270.
15. S. TSURUMI, T. IWATA, Y. TAJIMA and M. HIKITA, *Jpn J. Appl. Phys.* **26** (1987) L1865.
16. T. ITOH, M. UZAWA and H. UCHIKAWA, *J. Crystal Growth* **91** (1988) 397.
17. F. BERTAUT and C. DELORME, *C. R. Acad. Sci. Paris* **233** (1951) 356.
18. F. H. RHINES and J. S. WOLF, *Metall. Trans.* **1** (1970) 1701.
19. G. R. WALLWORK, "The Oxidation of Alloys", Reports on Progress in Physics, Vol. 39 (The Institute of Physics, London, 1976) p. 401.
20. G. L. LEATHERMAN, D. QUINN, R. K. MacCRONE and S. R. SHATYNSKI, in "Proceedings JIMIS-3 (1983) High Temperature Corrosion of Metals and Alloys", supplement to transactions of the Japan Institute of Metals, Vol. 24 (The Institute of Metals, Sendai, Japan, 1983) p. 149.
21. J. BULARZIK, P. K. DAVIES and A. NAVROTSKY, *J. Amer. Ceram. Soc.* **69** (1989) 453.

Received 17 June
and accepted 16 December 1991